Electronic Supplementary Material (ESI) for Nanoscale.

X-ray-triggered NO-released Bi–SNO nanoparticles: all-in-one nano-radiosensitizer with photothermal/gas therapy for enhanced radiotherapy

Fangmei Zhang[a], Shikai Liu[a], Na Zhang[b], Ye Kuang[a], Wenting Li[a], Shili Gai[a], Fei He[a], Arif Gulzar[a], and Piaoping Yang*[,a]

[a] Key Laboratory of Superlight Materials and Surface Technology, Ministry of Education, College of Materials Science and Chemical Engineering, Harbin Engineering University, Harbin, 150001, P. R. China.

[b] Drug Safety Evaluation Center, Heilongjiang University of Chinese Medicine, Harbin 150040, P. R. China

*Corresponding author
E-mail: yangpiaoping@hrbeu.edu.cn

Calculation of the Photothermal Conversion Efficiency

The photothermal conversion efficiency (η) is calculated as follows:

$$\eta = \frac{hS(T_{max} - T_{surr}) - Q_{dis}}{I(1 - 10^{A_\lambda})}$$

When η is the thermal conversion efficiency of the nanomaterial, S is the area of the sample, T_{max} represents the highest temperature (51.5°C) of the sample after irradiation. T_{surr} stands for the ambient temperature (25.6°C). Q_{dis} is the heat of the blank solvent, which is measured be 20.0 mW. A_λ is the absorbance value of the sample at the excitation wavelength λ (λ = 808 nm) and A means the absorption intensity of Bi-SNO NPs solution (300 μg mL^{-1}), and I is the laser power based on the equation (0.8 W/cm^2). hs can be applied the linear time date from the cooling period vs -In θ (Fig. 2e).

$$hs = \frac{mc}{k}$$

Figures

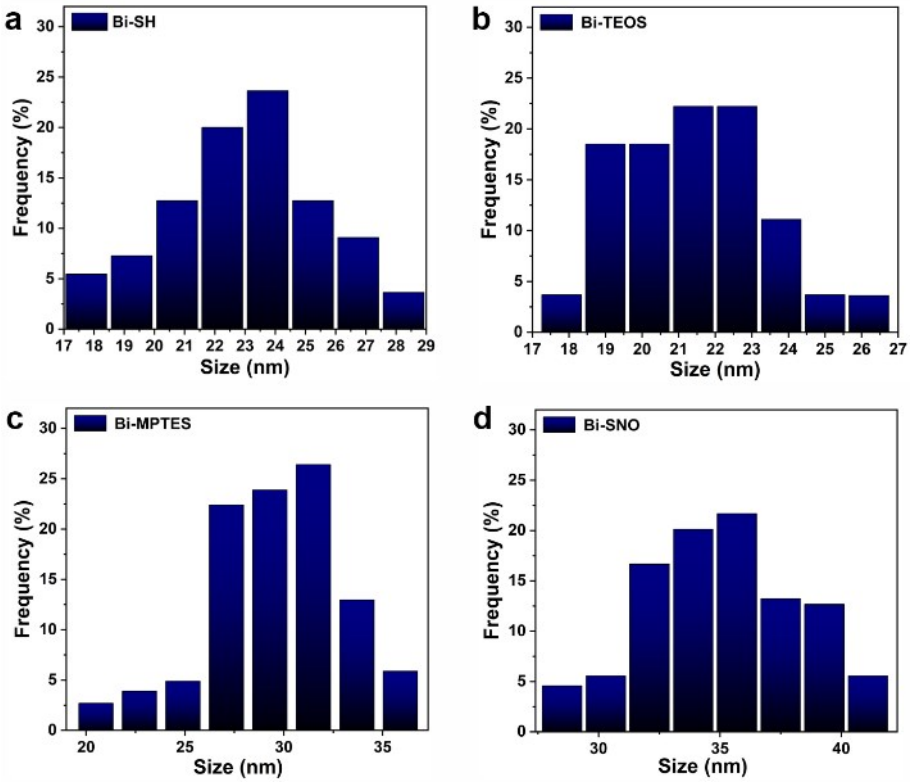

Fig. S1 The size distribution histograms of Bi-SH, Bi-TEOS, Bi-MPTES, and Bi-SNO NPs, respectively.

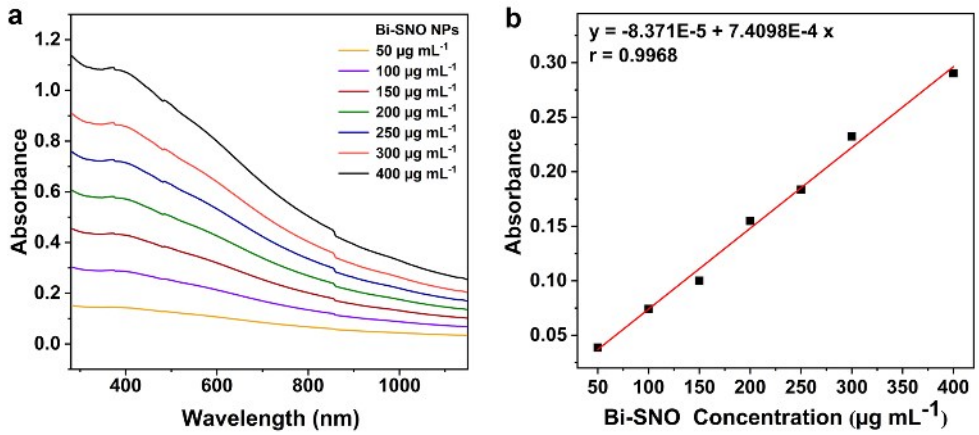

Fig. S2 (a): UV-vis absorbance spectra of Bi-SNO with different concentrations at room temperature. (b): A linear relationship for the optical absorbance at 808 nm as a function of Bi-SNO concentration (50, 100, 150, 200, 250, 300, and 400 μg mL^{-1}).

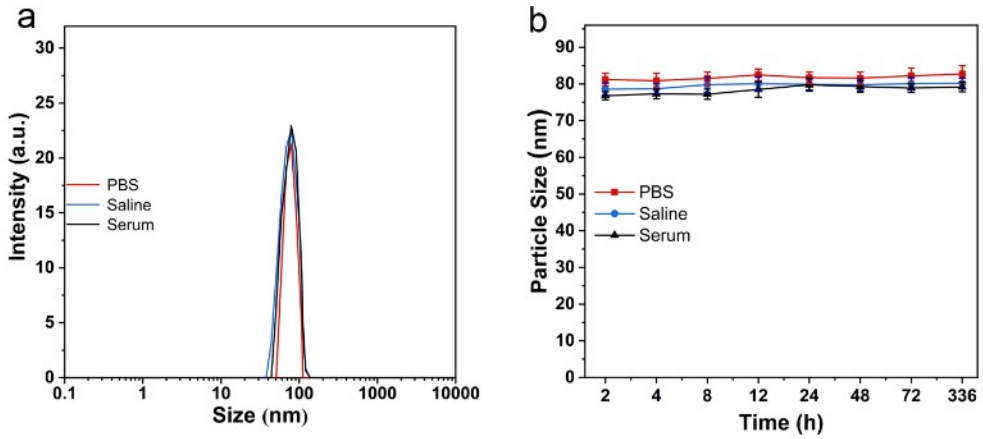

Fig. S3 (a) The particle size distributions of Bi-SNO NPs in different solvents (including phosphate buffered solution (PBS), saline, and serum) measured by dynamic light scattering (DLS). (b) The long-term stability of Bi-SNO NPs in various solvents throughout 14-day (336 h).

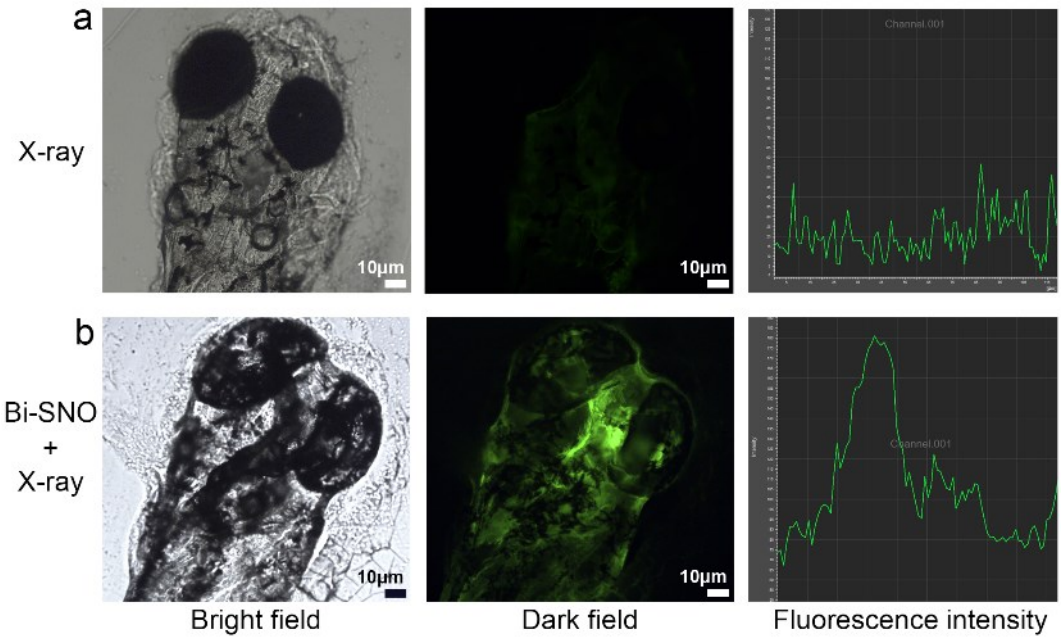

Fig. S4 X-ray triggered NO release from Bi-SNO in zebrafish larvae. (a) CLMS images of zebrafish incubated with DAF-FM-DA under 5 Gy radiation. (b) CLMS images of zebrafish incubated with Bi-SNO and DAF-FM-DA upon exposure to 5 Gy radiation.

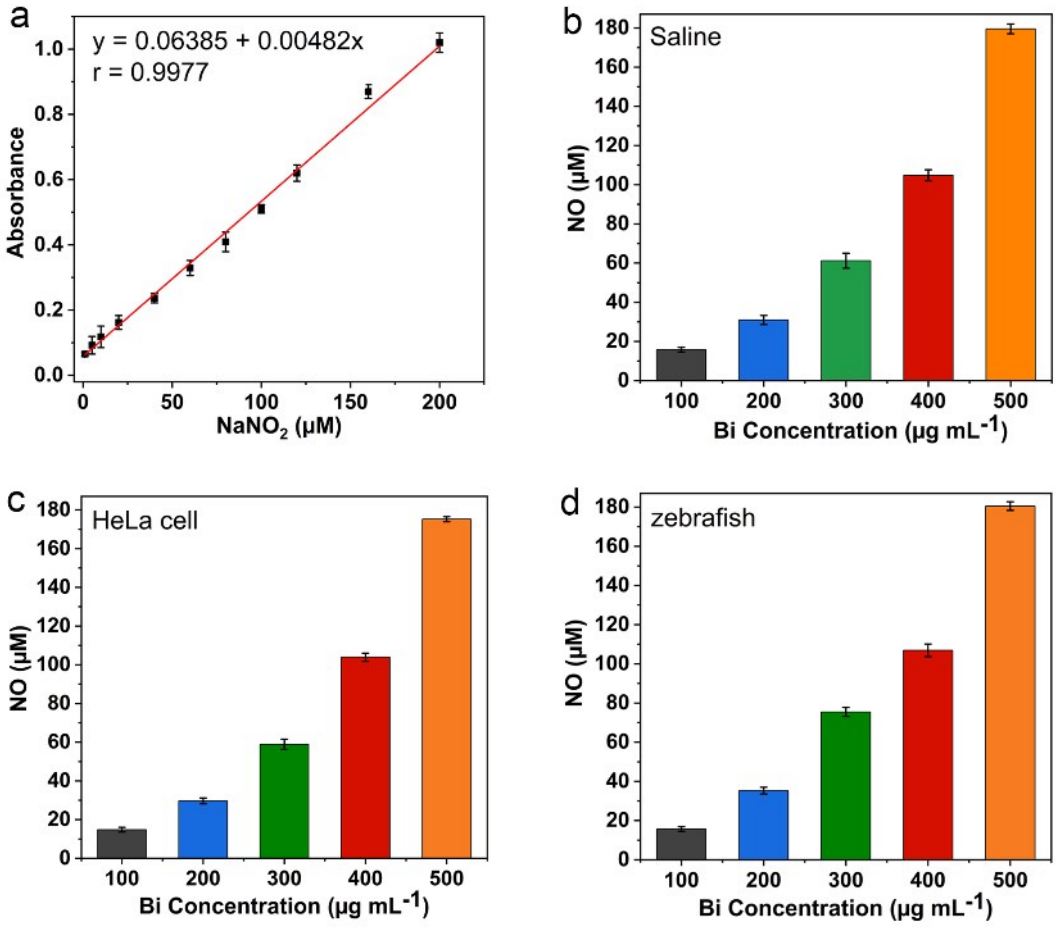

Fig. S5 (a) Calibration curve of absorbance at 540 nm versus the concentration of nitrite ($NaNO_2$). (b) Quantitative evaluation of NO release from various concentration of Bi-SNO in saline (b), HeLa cells (c), and

zebrafish (d) after exposure to X-ray radiation (5 Gy). All experiments were performed according to the Griess kit protocols.

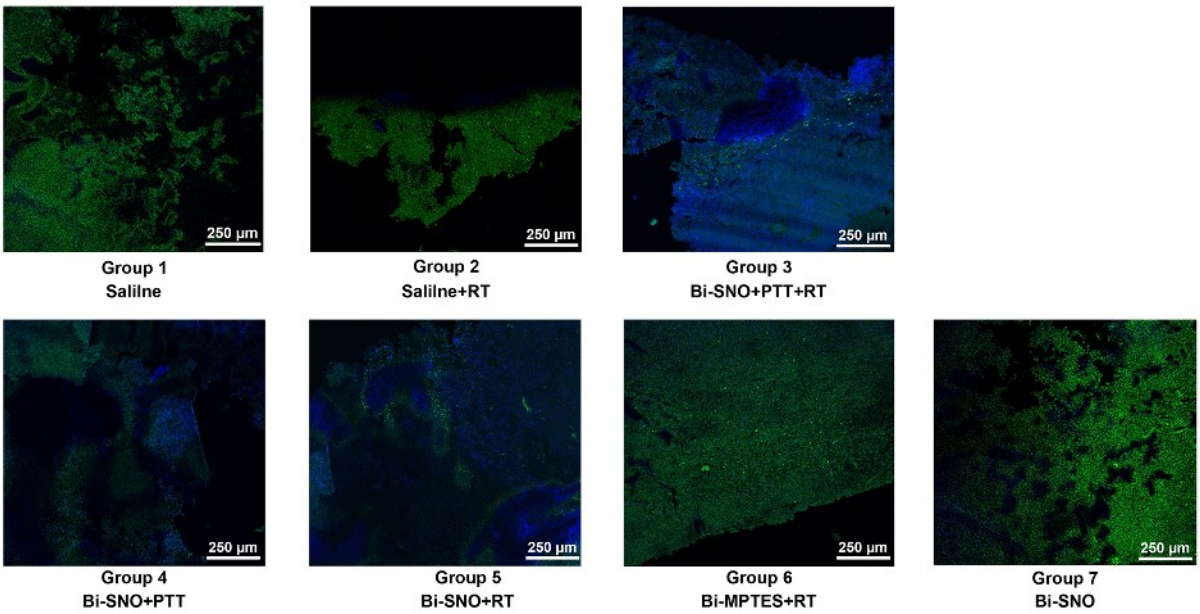

Fig. S6 Immunofluorescent staining of HIF-1α (hypoxia probe, green) and nuclei (DAPI, blue) of tumor slices after various treatment.

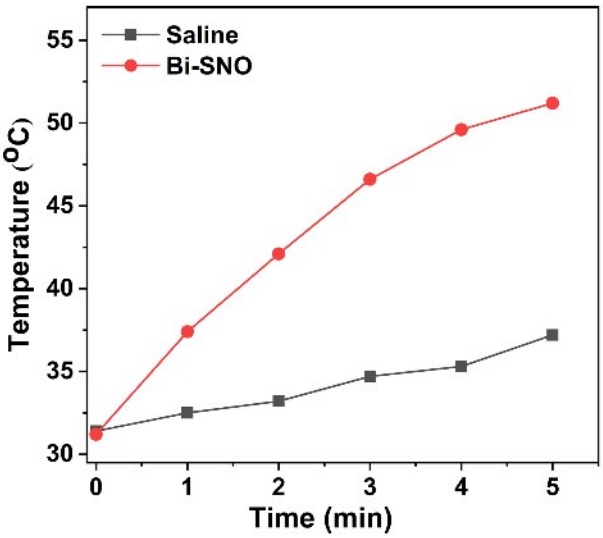

Fig. S7 Temperature change curves of tumor-bearing mice intratumorally injected with saline and Bi-SNO.